Chapter 6 SERS Application of MoS_2 Nanostructures

6.1 Introduction

Increasing industrialization is leading to discharge of different organic/inorganic pollutants in water resources and hence their detection and treatment is important for the survival of human society. Raman spectroscopy is a fast and non-destructive optical technique that can provide the characteristic information of the probe molecules/analytes and hence it has been widely used in different applications in chemistry, physics, and medicine in the last few decades [104, 196, 197]. This method allows the label free detection of organic compounds at very low concentration. Surface enhanced Raman spectroscopy (SERS) has been widely used in the last two decades for the detection of industrial waste, chemical, food industries and medical science. The SERS signal amplification occurs due to the interaction among the incident light, analyte molecule and the active SERS substrate (metallic or semiconducting surface). Among newly studied materials, 2D materials are found suitable for the SERS applications due to the layer-dependent optical properties, high surface to volume ratio and good stability [66]. Researchers developed 2D materials based active SERS substrates with different morphologies like flower, sheet etc. for the detection of organic pollutants. The chemically inert surface of 2D materials opposes the deformation and chemical reactions of the probe molecule with the surface and due to this, the reproducible enhancement is possible for quantitative analysis. The mechanism behind the SERS enhancement is an exciting area of science to investigate. Most of the researchers have commonly used two theories, electromagnetic (EM) enhancement and chemical (CM) enhancement. The two mechanisms are applicable to metallic and semiconducting substrates. The excitation of

localized surface plasmon resonance (LSPR) mode in metal substrates is known to be responsible for EM enhancement [198]. The LSPR occurs when the metal nanoparticle excites at the resonance frequency of the incident light. On the other hand, the CM enhancement happens due to the charge transfer between the probe molecule and semiconducting SERS substrate [143, 199]. A schematic representation of SERS process is given in **Figure. 6.1**. The roughness of active SERS substrate, adsorption of analyte molecules, wavelength of incident laser and interaction between analyte-substrate play important role in SERS detection of analyte.

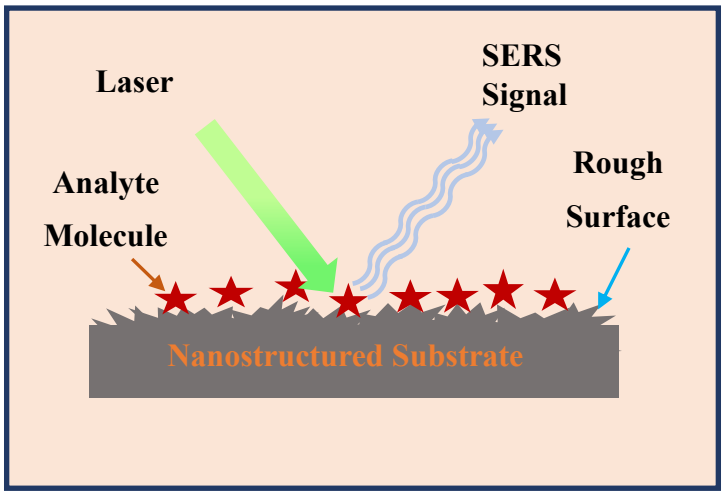

Figure. 6.1 *Schematic diagram of SERS process.*

The semiconducting MoS_2 can also be used as a substrate for SERS detection of organic/biological pollutants, present in the water. In literature, few studies on MoS_2 based SERS detection of organic molecules were performed. Zuo *et al*. discussed about the defect/active sites on MoS_2, which can enhance the charge transfer between MoS_2 and the probe molecule Rhodamine6G (R6G) and observed the limited chemical enhancement factor of 10 for pristine MoS_2 [200]. They created the defects on MoS_2 using femtosecond laser and increased the enhancement factor up to 63.5. Sun *et al*. discussed the layer dependent chemical enhancement of R6G molecule and observed that bulk

MoS_2 is not suitable for SERS application [111]. Anbazhagan *et al*. performed a comparative study between metallic and semiconducting phases of MoS_2 for SERS application [201]. In this chapter, we have discussed SERS enhancement for the detection of organic pollutants using CVD grown three different MoS_2 nanostructures. We have characterized the dye molecules (R6G and Methyl orange (MO)) via UV-Visible and Raman spectroscopy to identify the absorption peak position and characteristics Raman mode of the dye molecules. In the following section, we have discussed the SERS detection of R6G using horizontally grown interconnected network of few-layer MoS_2 on Si substrate and triangular bi-layer MoS_2 on SiO_2/Si substrate. The vertically oriented few-layer MoS_2 on Si substrate have been used for the detection of R6G and MO dyes.

6.1.1 Enhancement Factor (EF)

The quantification of SERS for probe molecule detection is done by Enhancement factor (EF), which is a pure number. The EF depends on the SERS substrate, excitation source and the analyte molecule and its value can be found anywhere in the range 10 - 10^{14} [202]. In case of SERS measurement, a diversity of situations can arise such as single molecule, multiple molecules, distribution of analyte molecule on the surface and the averages over time etc., which make a single general definition of the EF impossible in a SERS process [202]. Hence, there have been different ways of calculating EF as follows-

i. Single-Molecule Enhancement Factor (SMEF)

ii. Substrate Specific Enhancement Factor (SSEF)

iii. Analytical Enhancement Factor (AEF)

In order to quantify the SERS enhancement limit of prepared MoS_2 nanostructures in the present work for the detection of R6G and MO, we have calculated the analytical enhancement factor (AEF), which signifies that how much SERS signal enhances under

given experimental conditions as compared to the normal Raman. It can be described as follows

$$AEF = \frac{I_{SERS}/C_{SERS}}{I_{RS}/C_{RS}} \quad (6.1)$$

where C_{RS} is the concentrations of the analyte and I_{RS} is the normal Raman signal under non-SERS condition. C_{SERS} is the lowest detected concentration of the same analyte, which produces SERS signal of intensity I_{SERS} under same conditions like excitation wavelength and laser power, objective lens and spectrometer etc [202].

6.1.2 Mechanism for SERS Signal using MoS_2 Substrates

The prepared MoS_2 nanostructures are semiconducting in nature and hence in order to understand the reason behind the signal enhancement for MoS_2 as SERS substrate, we need to look into the semiconductor-molecule system. In this system, mainly three resonances contribute to the SERS signal enhancement, which are exciton resonance, molecular resonance and charge transfer [203]. The intensity of a Raman transition depends on the polarizability tensor of the materials in the following form [135, 144, 203] -

$$I = [8\pi(\omega \pm \omega_{I'I})^4 I_L / 9C^4] \sum \alpha_{\sigma\rho}^2 \quad (6.2)$$

where I_L is the intensity of laser at angular frequency ω and the molecular transition frequency is $\omega_{I'I}$ between states I and I′. The term 'α' is the polarizability of the molecule and the three directions in space (X, Y, Z) are represented by subscripts σ and ρ. The polarizability (α) of the molecule is the sum of the three terms and expressed as [203] -

$$\alpha_{\sigma\rho} = A + B + C \quad (6.3)$$

The charge-transfer transitions moment μ_{IC} represents the charge transfer from HOMO level to the conduction band edge C of the semiconductor. Similarly, transition moment μ_{VK} represents the charge transfer transitions from valence band edge V to the molecule LUMO level. The charge transfer can borrow the intensity either from the molecular transitions μ_{KI} or from the excitation transitions μ_{VC}. The SERS intensity is proportional to $|R|^2$ and the A, B and C terms can be expressed as follows [203] -

A-Term: This term can be written as

$$R_{IC}(\omega) = \frac{\mu_{IC}\mu_{IC}\langle i|k\rangle\langle k|f\rangle}{((\varepsilon_1(\omega)+2\varepsilon_0)^2+\varepsilon_2^2(\omega))((\omega_{IC}^2-\omega^2)+\gamma_{IC}^2)} \tag{6.4}$$

$$R_{VK}(\omega) = \frac{\mu_{VK}\mu_{VK}\langle i|k\rangle\langle k|f\rangle}{\left((\varepsilon_1(\omega)+2\varepsilon_0)^2+\varepsilon_2^2(\omega)\right)\left((\omega_{VK}^2-\omega^2)+\gamma_{VK}^2\right)} \tag{6.5}$$

where the real and imaginary parts of the permittivity of the materials are ε_1 and ε_2. The ε_0 is the permittivity of free space and γ is the damping factor. The first term in both the equations in the denominator is the plasmon resonance term. The resonance terms in the above equations can occur via charge transfer either from HOMO level to conduction band edge (at $\omega = \omega_{IC}$) or the valance band edge to the LUMO level (at $\omega = \omega_{VK}$).

B-Term and C-Term:

The B term can be expressed as-

$$R_{ICK}(\omega) = \frac{\mu_{KI}\mu_{IC}h_{CK}\langle i|Q_k|f\rangle}{((\varepsilon_1(\omega)+2\varepsilon_0)^2+\varepsilon_2^2(\omega))((\omega_{IC}^2-\omega^2)+\gamma_{IC}^2)((\omega_{KI}^2-\omega^2)+\gamma_{KI}^2)} \tag{6.6}$$

$$R_{ICV}(\omega) = \frac{\mu_{VC}\mu_{IC}h_{IV}\langle i|Q_k|f\rangle}{((\varepsilon_1(\omega)+2\varepsilon_0)^2+\varepsilon_2^2(\omega))((\omega_{IC}^2-\omega^2)+\gamma_{IC}^2)((\omega_{VC}^2-\omega^2)+\gamma_{VC}^2)} \tag{6.7}$$

The B term explains the charge transfer from the molecule to the semiconductor. This term explains the charge-transfer resonance coupled with molecular resonance via Herzberg-Teller constant. The B term is obtained from charge transfer from molecular

HOMO level to the CB edge at $\omega = \omega_{IC}$. The large enhancement occurs when it happens at molecular transition at $\omega = \omega_{IK}$ or exciton transition at $\omega = \omega_{VC}$. The h_{IV} and h_{CK} are the Herzberg−Teller vibronic coupling terms involved in charge transfer process [135, 203].

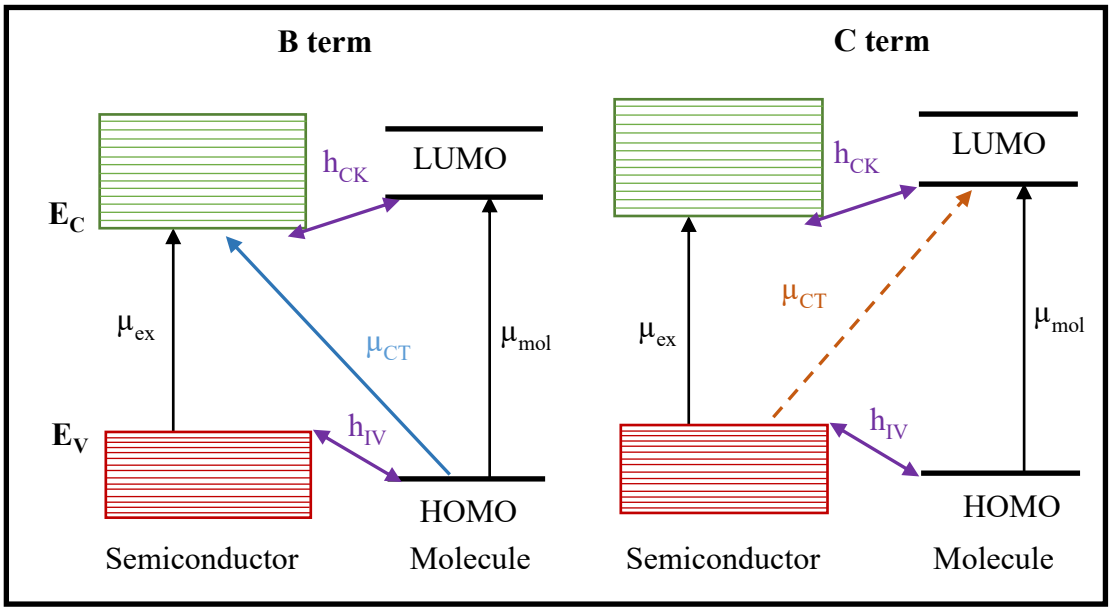

Figure. 6.2 *The coupling diagram for B-term and C-term in semiconductor-molecule system [36].*

The C term can be expressed as-

$$R_{IVK}(\omega) = \frac{\mu_{VK}\mu_{KI}h_{IV}\langle i|Q_k|f\rangle}{\left((\varepsilon_1(\omega)+2\varepsilon_0)^2+\varepsilon_2^2(\omega)\right)\left((\omega_{VK}^2-\omega^2)+\gamma_{VK}^2\right)\left((\omega_{KI}^2-\omega^2)+\gamma_{KI}^2\right)} \tag{6.8}$$

$$R_{KVC}(\omega) = \frac{\mu_{CV}\mu_{VK}h_{KC}\langle i|Q_k|f\rangle}{\left((\varepsilon_1(\omega)+2\varepsilon_0)^2+\varepsilon_2^2(\omega)\right)\left((\omega_{VK}^2-\omega^2)+\gamma_{VK}^2\right)\left((\omega_{CV}^2-\omega^2)+\gamma_{CV}^2\right)} \tag{6.9}$$

The C term explains the charge transfer from the semiconductor to the molecule. The schematic representation of different transitions involved in B and C terms of **equation 6.3** is given in **Figure 6.2**. It explains the charge transfer from VB edge to molecular LUMO level. In the case of semiconductor-molecular system, the enhancement occurs when molecular transitions (at $\omega = \omega_{IK}$) or an exciton transition (at $\omega = \omega_{CV}$) is coupled

with other resonance via Herzberg-Teller coupling (h_{CK} or h_{IV}). The intensity is borrowed from either molecular transition (**equation-6.6**) or exciton transition (**equation-6.7**), as shown in **Figure 6.2**.

6.2 Results and Discussion

6.2.1 Characterization of Dye Molecules

Rhodamine 6G (R6G) and Methyl Orange (MO) dyes have been chosen for SERS detection. The photographs of R6G and MO dyes at two different concentrations (10^{-3} M and 10^{-6} M) are shown in **Figure 6.3**. The aqueous solutions of R6G and MO of micro molar or lower concentrations become colourless and hence at these concentrations they cannot be detected via UV-vis spectroscopy.

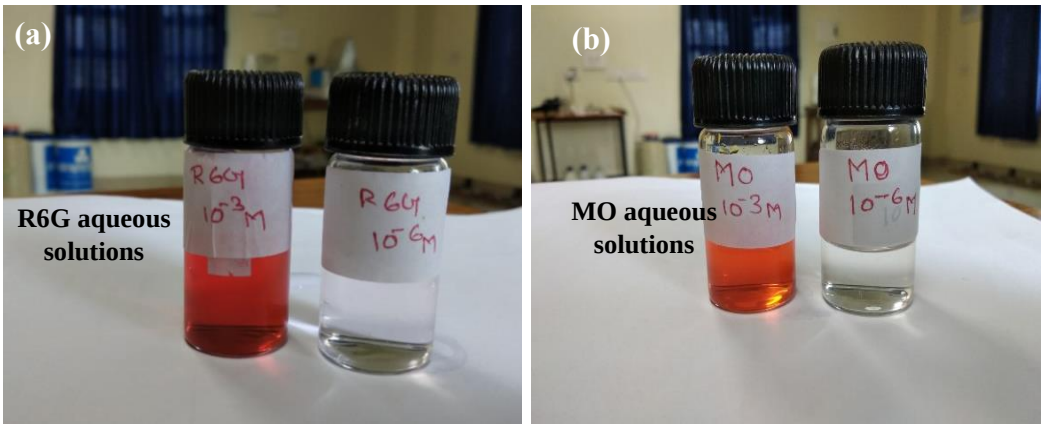

Figure 6.3 *The photograph of aqueous solutions of (a) R6G and (b) MO dye at two different concentrations.*

The UV-visible spectra of the R6G and MO molecules at 10^{-4} M concentrations in aqueous medium are shown in **Figure 6.4 (a)** and **Figure 6.4 (b)**, respectively. The UV-visible spectrum of R6G shows a strong absorption peak at around 525 nm, while UV-visible spectrum of MO shows absorption around 467 nm. The Tauc plot of R6G molecule is shown in **Figure 6.4 (c)**, indicating the optical bandgap for R6G molecule around 2.27 eV. The MO molecule having a broad peak around 467 nm and the

corresponding Tauc plot is shown in **Figure 6.4 (d)**, indicating corresponding optical bandgap around 2.21 eV. The absorption peak of R6G is in close resonance with SERS laser source (532 nm), while MO is also having significant absorption in similar range. This suggests that SERS signal may be enhanced due to the molecular resonance.

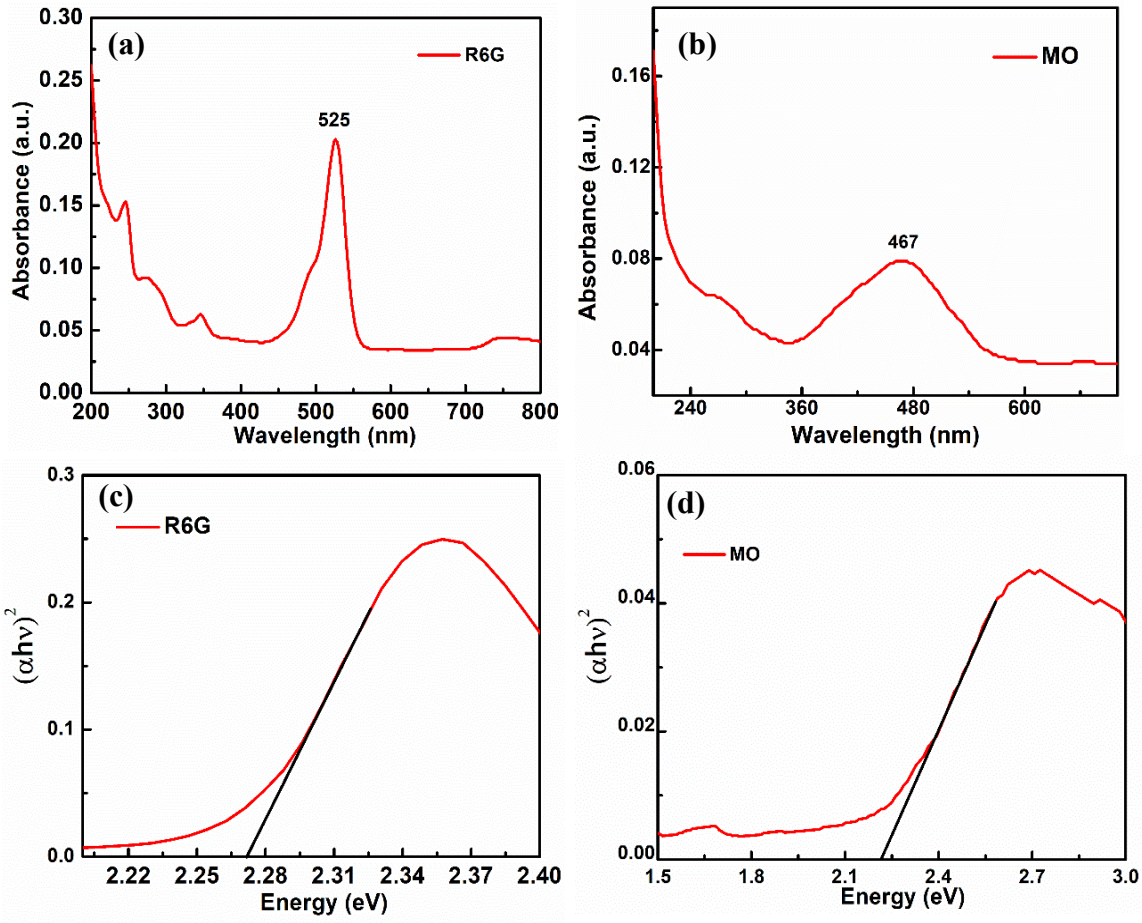

Figure 6.4 *UV-Vis spectra of (a) R6G in DI water and (b) MO in DI water (c) Corresponding Tauc plot of R6G. (d) Corresponding Tauc plot of MO.*

To find the characteristic Raman peaks of the R6G and MO molecule, we performed their Raman spectra in powder form. The Raman spectra of bulk R6G and MO molecules are shown in **Figure 6.5 (a)** and **Figure 6.5 (b),** respectively**,** indicating the characteristic peaks of both the dye molecules. The Raman peak of R6G at ~ 1195 cm^{-1} corresponds to C-H in-plane bending of R6G, while other peaks (at 1368, 1570, 1533 and 1650 cm^{-1}) correspond to the stretching vibrations for aromatic C-C. The peak at 611 cm^{-}

^{1} corresponds to the in-plane bending mode of C-C-C ring and 770 cm^{-1} belongs to the C-H out-of-plane bending mode for R6G [204]. The Raman peaks of MO molecule at 1390 and 1418 cm^{-1} are associated with N=N stretching vibration. The Raman peaks around 1591, 1445 and 1312 cm^{-1} correspond to the C–C stretching vibration, while peaks at 1195 and 1117cm^{-1} belongs to the Ph-N stretching vibration of MO. The peak at 1145 cm^{-1} is due to the C-H vibration and peak at 923 cm^{-1} corresponds to the bending mode of C-H and C-C [205].

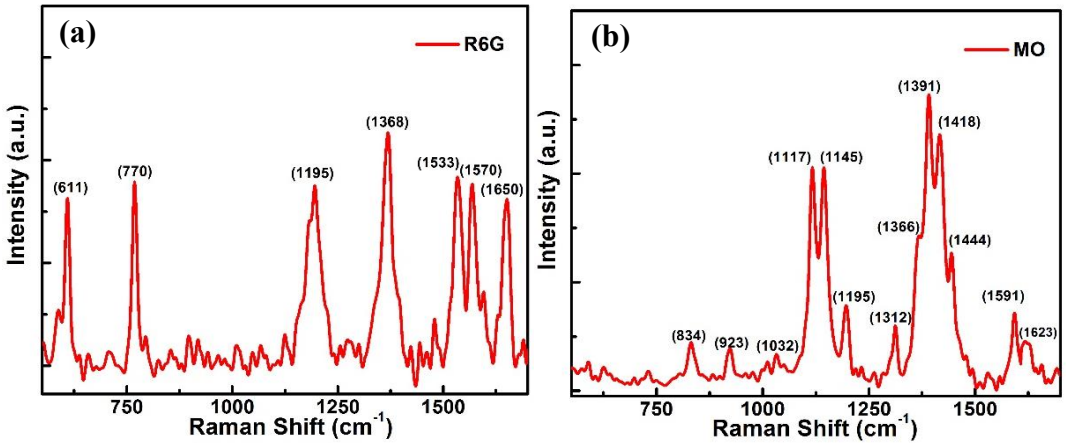

Figure 6.5 *Raman spectra of (a) Bulk R6G and (b) Bulk MO on glass slide.*

6.2.2 SERS Application of Horizontally Grown Interconnected Network of Few-Layer MoS_2

The surface morphology (using SEM) of the horizontally grown interconnected network of few-layer MoS_2 is shown in **Figure 6.6 (a)**. The AFM image and corresponding height profile for interconnected network of few-layer MoS_2 has been already discussed in **Figure 5.2** of **chapter 5**, which indicates presence of 5 to 6 layers with total thickness around 4 nm and surface roughness around 1 nm. Surface roughness provides more accessible surface area in given length scale and hence this few-layer MoS_2 can be used for SERS detection. In order to realize the detection of R6G molecule at very low concentration, we used the interconnected networks of few-layers MoS_2 over

Si as SERS substrate. SERS spectrum with R6G (10^{-6} M) is shown in **Figure 6.6 (b)** indicating characteristic peaks of MoS_2 (E^1_{2g} ~ 382.2 cm^{-1} and A_{1g} ~ 406.4 cm^{-1} peaks), Si (~520 cm^{-1}) and R6G. The separation of around 24.2 cm^{-1} between characteristic modes of MoS_2 suggests presence of around 5 to 6 layers in few-layers MoS_2, as observed in AFM analysis [190].

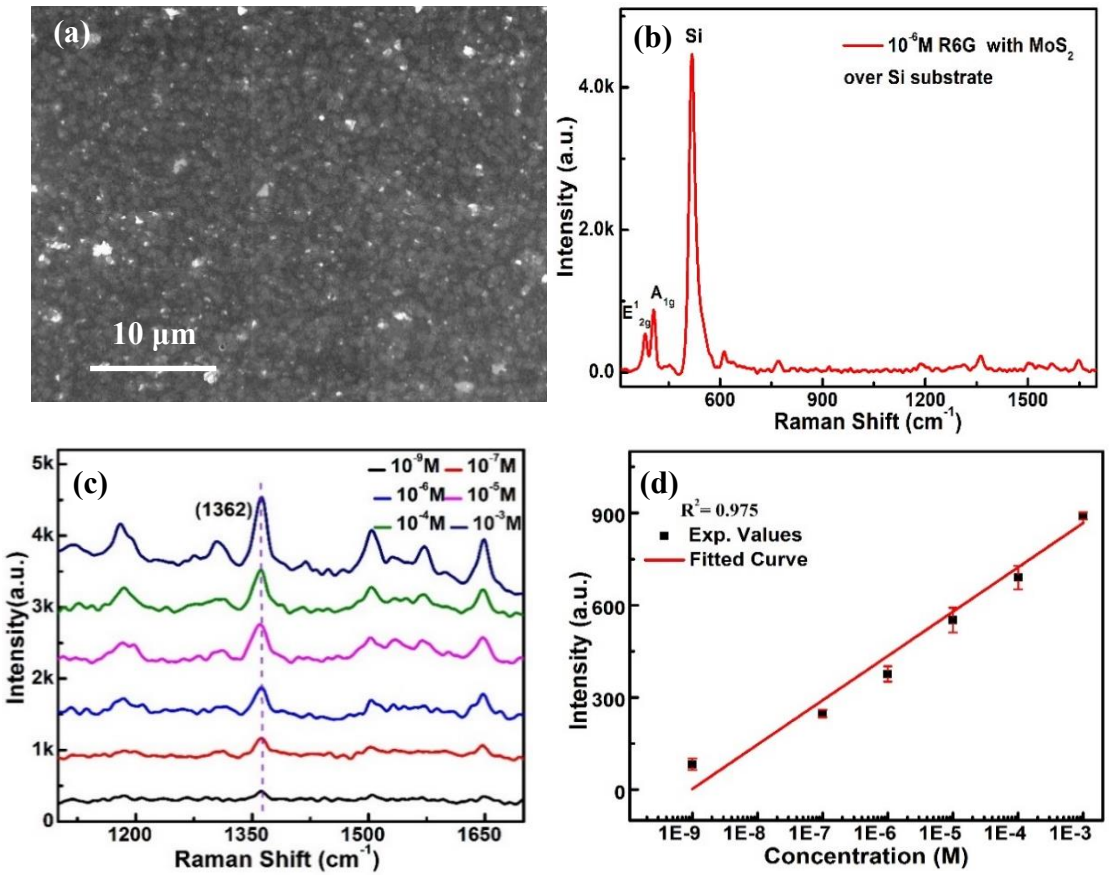

Figure 6.6 *(a) SEM image of few-layer MoS_2/Si substrate, (b) SERS spectrum showing characteristic peaks of MoS_2, Si and R6G, (c) SERS spectra of R6G molecules on interconnected network of few-layer MoS_2/Si substrate at different concentrations (10^{-3} to 10^{-9} M), (d) Raman intensity of 1362 cm^{-1} peak for R6G as a function of the R6G concentrations.*

Varying ultralow concentrations (10^{-3} to 10^{-9} M) of R6G molecules have been prepared for SERS detection. SERS signals of interconnected network of few-layer MoS_2/Si substrate, dipped in different concentrations of R6G, are shown in **Figure 6.6 (c)**. The peak positions in SERS spectra of R6G are found shifted compared to Raman

spectra of bulk R6G, indicating the interaction between R6G and SERS substrate. **Figure 6.6 (c)** clearly indicates that the intensities of different Raman peaks are increased with increasing concentrations, as indicated in linear plot of **Figure 6.6 (d)**. It shows the variation of intensity of peak at 1362 cm^{-1} with respect to different concentrations of R6G molecules. In order to calculate the enhancement factor, a Raman peak of R6G at 1362 cm^{-1} has been chosen, which corresponds to aromatic C-C stretching of R6G. The intensities of the SERS spectra of R6G molecules are proportional to the logarithm of the concentrations of the R6G molecule in distilled water. The good linear response of SERS is obtained from 1 nM to 1 mM concentrations. The linear fitted curve of **Figure 6.6 (d)** can be used for quantitative detection in terms of AEF for R6G using interconnected network of few-layer MoS_2/Si substrate. A reference Raman spectrum of R6G molecules (10^{-3} M) over pure Si substrate is shown in **Figure 6.7**.

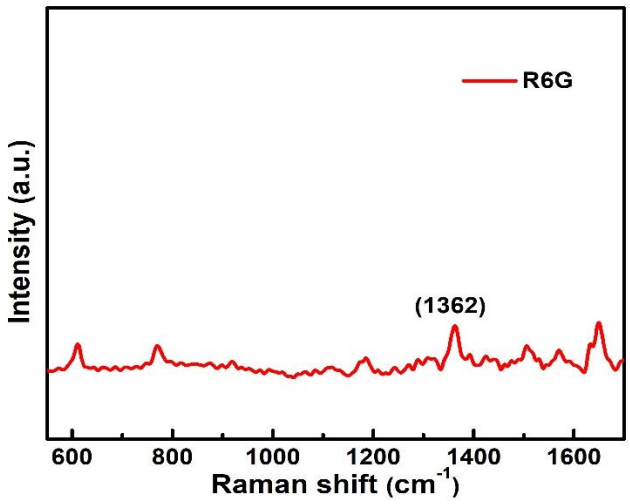

Figure 6.7 *Raman spectra of R6G molecules (10^{-3} M) on Si substrates.*

The enhancement in the Raman signal of R6G at low concentrations using SERS substrate is observed. The AEF for detection of R6G molecules has been calculated using **equation 6.1** and is found around 7.68×10^{2}. This signal enhancement can be attributed to the chemical interaction due to charge transfer process occurring between

semiconducting few-layer MoS_2 and R6G molecules [200]. This could be possible because of the surface roughness of prepared few-layers MoS_2, which lead to the better adsorption of R6G and hence better charge transfer between substrate and analyte to achieve higher detection limit. This could be explained through the schematic presentation of charge transfer process (coupling diagram for B-term and C-term) as shown in **Figure 6.2**. The electron-hole pairs are generated in HOMO-LUMO of R6G and valence-conduction band of few-layer MoS_2 under laser illumination. The presence of few-layer in MoS_2 may reduce recombination rate of charge carriers in MoS_2, which will further lead to reduction in difference between chemical potentials of R6G and few-layer MoS_2 [120]. Transfer of charge carriers may lead to higher number of electrons in excited states at MoS_2/R6G interface and hence may lead to higher intensity of Raman signals even at very low concentration of R6G (nanomolar concentrations). The efficient SERS detection may be attributed to the Herzberg-Teller vibronic coupling of various resonances in analyte/MoS_2 system, mainly comprising of three distinct processes: (i) molecular resonance due to laser excitation; (ii) excitonic resonance and (iii) surface interactions between the molecule and the substrate [112, 203].

6.2.3 SERS Application of Horizontally Grown Triangular Bi-Layer MoS_2

The optical image of the horizontally grown triangular bi-layer MoS_2 film over SiO_2/Si substrate for SERS application is shown in **Figure 6.8 (a)**. We observe that the grown films are triangular in shape and the dimensions of each triangular structure is varying in the range 10 to 20 μm. The AFM image of triangular bi-layer MoS_2 is shown in **Figure 6.8 (b)** and its thickness is found around 1.6 nm, as shown in **Figure 6.8 (c)** indicating the presence of two layers. **Figure 6.8 (d)** shows the SERS spectrum of R6G (10^{-6} M) on triangular MoS_2 indicating characteristics peaks of MoS_2 (E^1_{2g} ~ 384.5 cm^{-1}

and A_{1g} ~ 405 cm^{-1} peaks), Si (~520 cm^{-1}) and R6G. The separation of ~20.5 cm^{-1} between two peaks of MoS_2, indicates the presence of two layers in MoS_2 [14, 153].

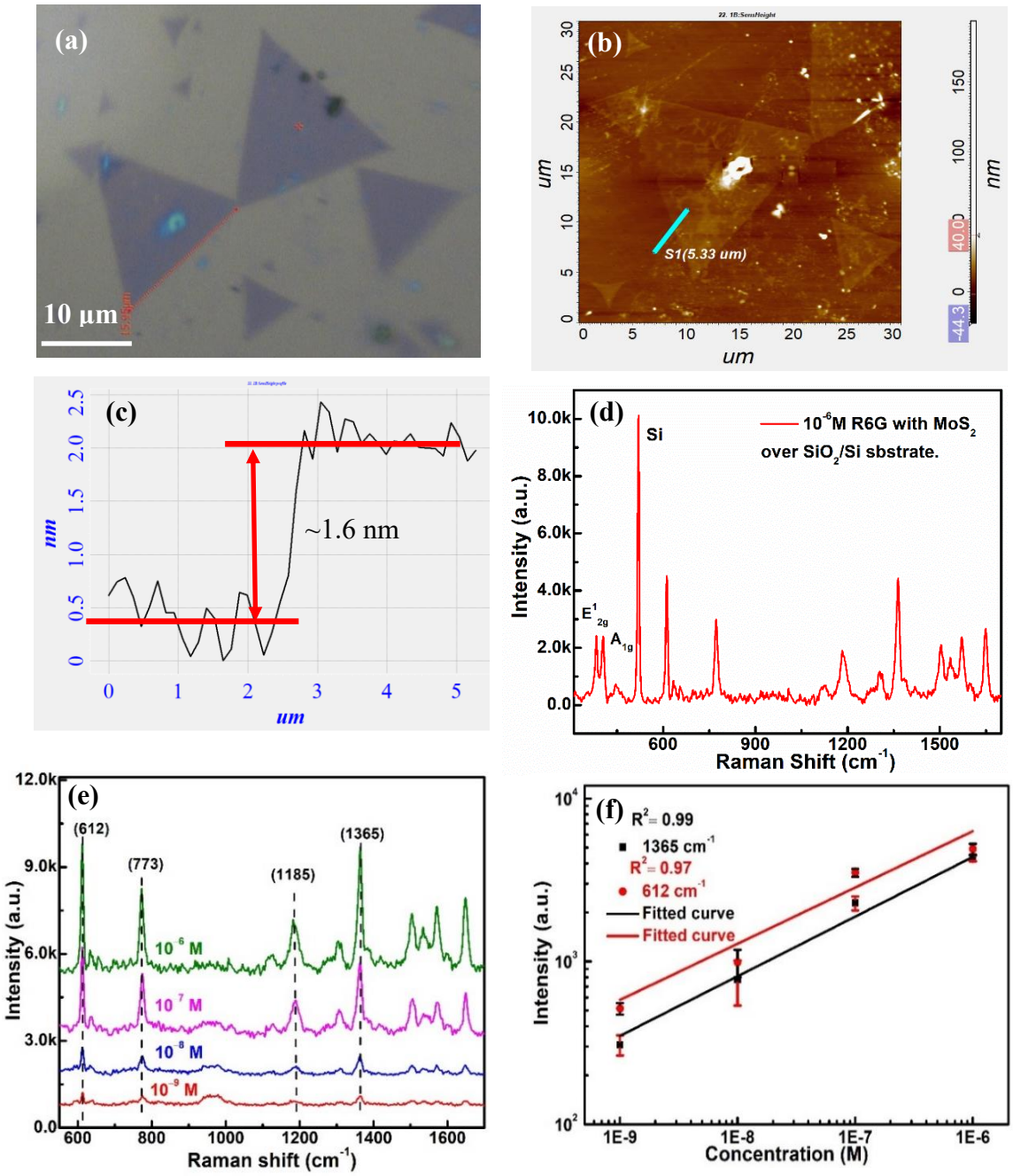

Figure 6.8 *(a) Optical image, (b) AFM image and (c) Corresponding height profile of triangular bi-layer MoS_2. (d) Full range SERS spectrum and (e) SERS spectra at different concentrations 10^{-6} - 10^{-9} M of R6G molecules on triangular bi-layer MoS_2 over SiO_2/Si substrates with (f) Raman intensity of 612 and 1365 cm^{-1} peaks for R6G as a function of the concentration of R6G.*

The SERS signals for R6G molecules adsorbed over the surface of triangular bi-layer MoS_2 over SiO_2/Si substrate at different concentrations (10^{-6} to 10^{-9} M) are shown in **Figure 6.8 (e)**. A significant shift in peak positions compared to Raman spectrum of bulk R6G and increased intensities of R6G modes are observed, suggesting the surface interaction between triangular bi-layer MoS_2 nanosheets and the analyte molecule R6G. The SERS peak intensity of all the peaks corresponding to R6G increases with the dye concentrations. Nearly linear response of two peaks (612 and 1365 cm^{-1}) intensities with dye concentration can be seen in **Figure 6.8 (f)**. The efficient SERS detection in semiconducting triangular bi-layer MoS_2 may be attributed to the Herzberg-Teller vibronic coupling with molecular and excitonic resonances, as shown schematically in **Figure 6.2**. In order to quantify the enhancement in SERS signal, AEF of triangular bi-layer MoS_2/SiO_2-Si SERS substrate for the detection of R6G molecules has been calculated using **equation 6.1**. The reference Raman spectrum of R6G molecule (10^{-3} M) on pure SiO_2/Si substrate is shown in **Figure 6.9**. The high value of AEF is achieved (around 3.07×10^3) due to efficient charge transfer process between substrate and analyte molecule through similar mechanism as described previously in **Figure 6.2** [135].

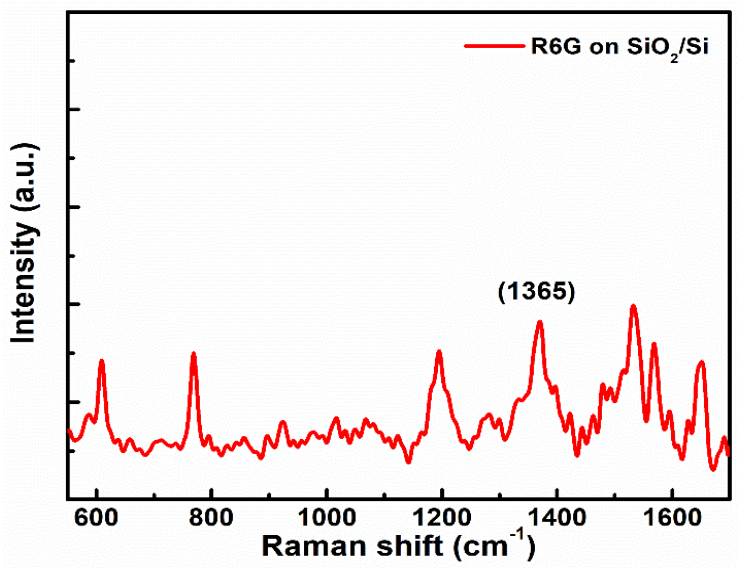

Figure 6.9 *Raman spectra of R6G molecules (10^{-3} M) on SiO_2/Si substrates.*

6.2.4 SERS Application of Vertically Oriented Few-Layer MoS_2

We also used vertically grown few-layer (VFL) MoS_2 over Si as SERS substrate for the detection of two dyes R6G and MO. The prepared SERS substrate was characterized by microscopy, X-ray diffraction and spectroscopy techniques. The SEM micrograph (**Figure 6.10 a**) shows the large area of interconnected MoS_2 nanosheets grown in vertical direction to the Si substrate. **Figure 6.10 (a)** clearly indicates the presence of large number of thin exposed edges of MoS_2, which can help in improving the light absorption and dye adsorption in SERS substrate. The crystalline nature of synthesized MoS_2 nanosheets has been studied by XRD pattern recorded in the 2θ range of 5° to 70° with a scan rate of 2° per minute. The XRD pattern with Le-Bail fitting for prepared VFL-MoS_2 nanosheets is shown in **Figure 6.10 (b)**. It clearly shows four major peaks at 2θ values of 14.37°, 28.98°, 44.09°, and 60.06°, corresponding to the (002), (004), (006) and (008) planes, respectively, for hexagonally symmetric 2H phase of MoS_2 with space group $P6_3/mmc$ (JCPDS card No. 37-1492). All these peaks are observed to be oriented in a common direction [001]. The calculated lattice parameters (a, b, c) from XRD analysis are a=b= 3.16 Å, c= 12.31 Å and α=β= 90°, γ=120° with unit cell volume V = 106.81 $Å^3$. The Raman spectrum of prepared MoS_2 nanosheets (**Figure 6.10 (c)**) indicates the presence of two characteristics optical phonon modes (E^1_{2g} ~ 384 cm^{-1} and A_{1g} ~ 409 cm^{-1}) corresponding to pure 2H phase of MoS_2 and a peak for Si substrate. The separation between two peaks of MoS_2 (~25 cm^{-1}) suggests the presence of few-layers in grown MoS_2 [96]. Additionally, a weak broad peak is observed around 453 cm^{-1} attributed to 2LA(M), a second-order Raman mode due to longitudinal acoustic (LA) phonons at the M point in the Brillouin zone [206]. Further, the semiconducting nature of prepared MoS_2 nanosheets was analyzed by PL study. The room temperature PL spectrum of MoS_2 nanosheets is shown in **Figure 6.10 (d)**, indicating the presence of A (~678 nm) and B (-

638 nm) excitons (peak positions via Gauss fitting) due to direct excitonic transitions at K point of Brillouin zone.

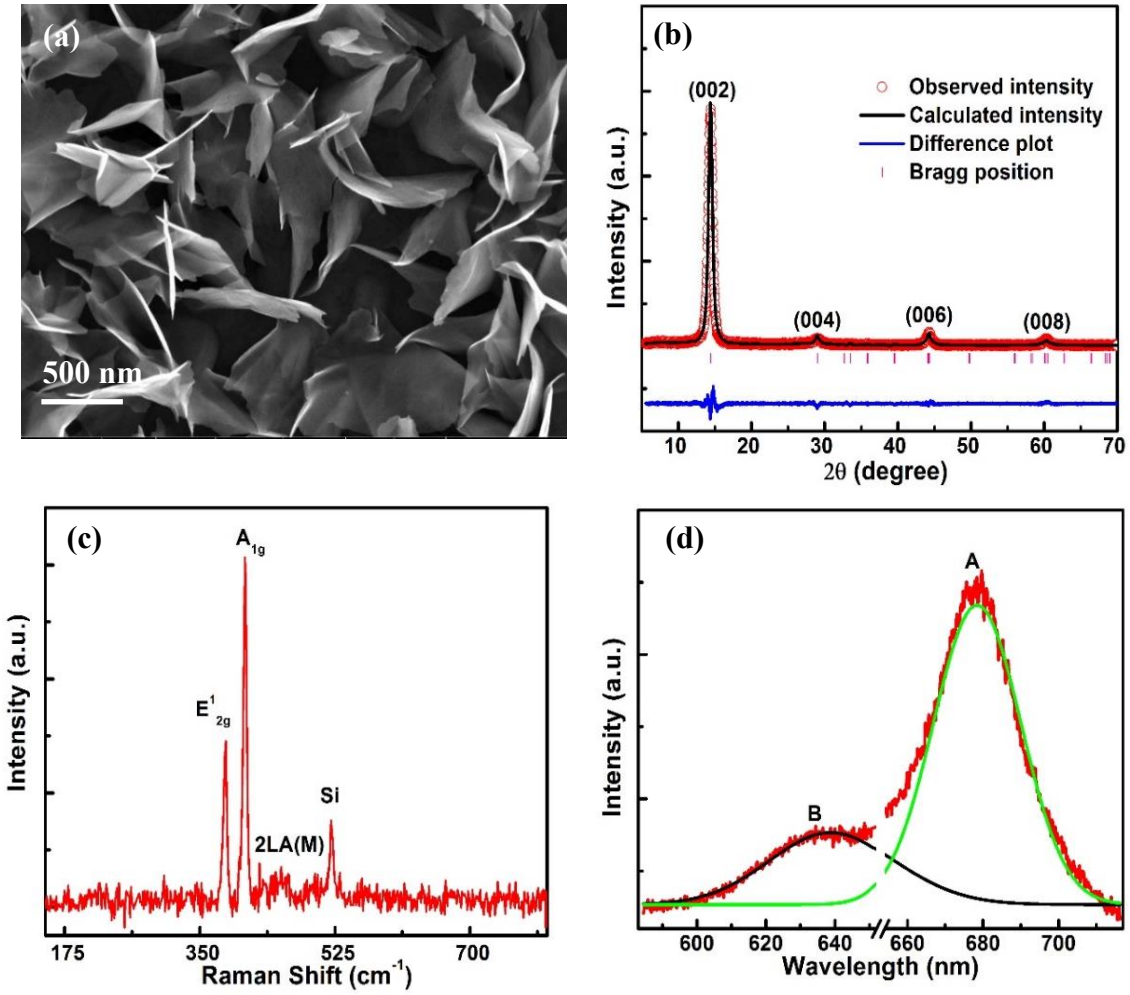

Figure 6.10 *(a) SEM image, (b) Le-Bail fitting of XRD pattern, (c) Raman spectrum and (d) Room temperature PL spectrum (Gauss fitted) of VFL-MoS_2.*

Figure 6.11 (a) and **Figure 6.11 (b)** show the SERS signals of R6G and MO molecules, respectively, adsorbed over the surface of MoS_2/Si at 10^{-6} M concentrations. They indicate the characteristics peaks of MoS_2 (E^1_{2g} and A_{1g}), Si substrate and respective dye molecule. In order to calculate AEF, reference Raman spectra of R6G and MO molecules (10^{-3} M) on pure Si substrate has been taken under same condition and are provided in **Figure 6.11 (c)** and **Figure 6.11 (d)**, respectively.

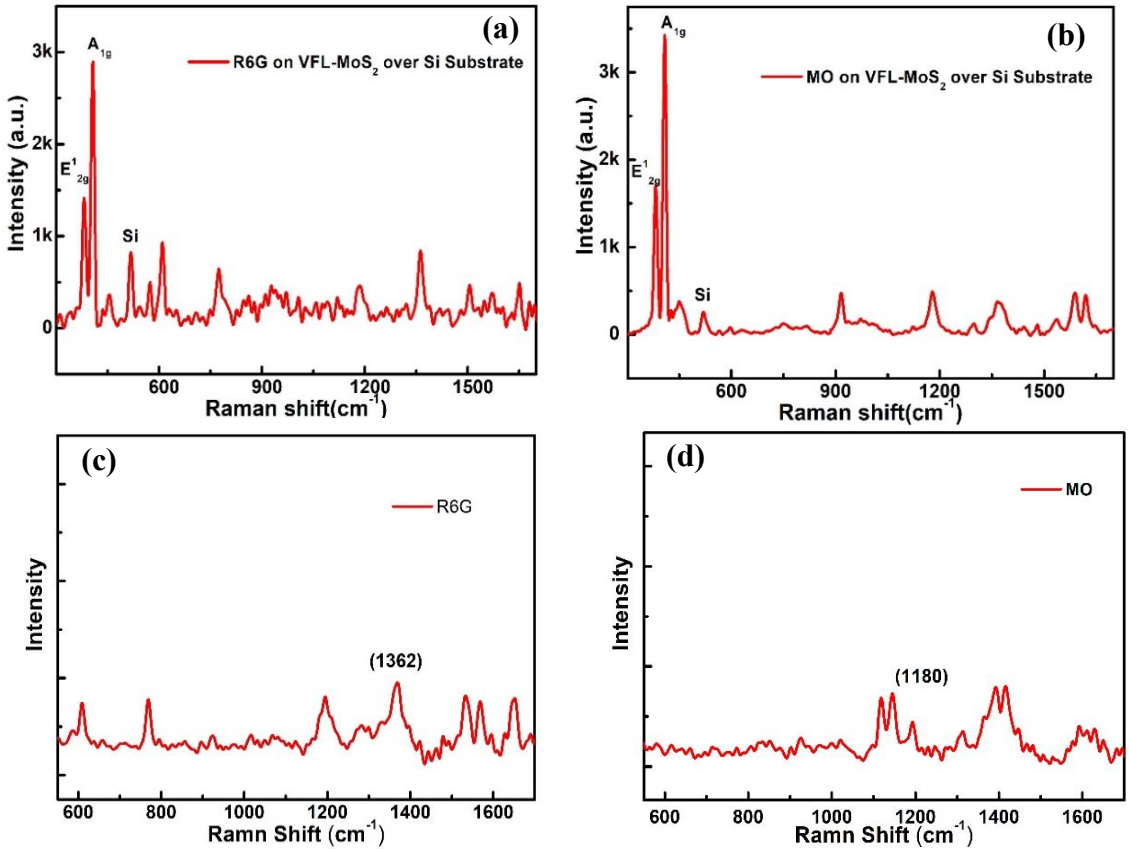

Figure 6.11 *SERS spectra of (a) R6G molecules and (b) MO molecules over VFL-MoS_2 on Si substrate.* (c) *SERS of R6G molecule and (d) SERS of MO molecule on pure Si substrates.*

SERS signals for R6G molecules adsorbed over the surface of VFL-MoS_2/Si at different concentrations (10^{-6} to 10^{-10} M) are shown in **Figure 6.12 (a)**. A significant shift and increased intensities of R6G modes are observed indicating the surface interaction between prepared VFL-MoS_2 nanosheets and R6G molecules. The high-intensity peaks at 611 and 1362 cm^{-1} are chosen for the detection of R6G in the present case. Nearly linear response of both the peaks intensities with dye concentration is shown in **Figure 6.12 (b)**. Similarly, SERS signals for MO on VFL-MoS_2/Si surface at different concentrations (10^{-6} to 10^{-10} M) are shown in **Figure 6.12 (c)**, which indicates significant shift and increased intensities of MO modes with concentration. The linear variation of intensity for peaks (1180 and 1620 cm^{-1}) with dye concentration is shown in **Figure 6.12 (d)**.

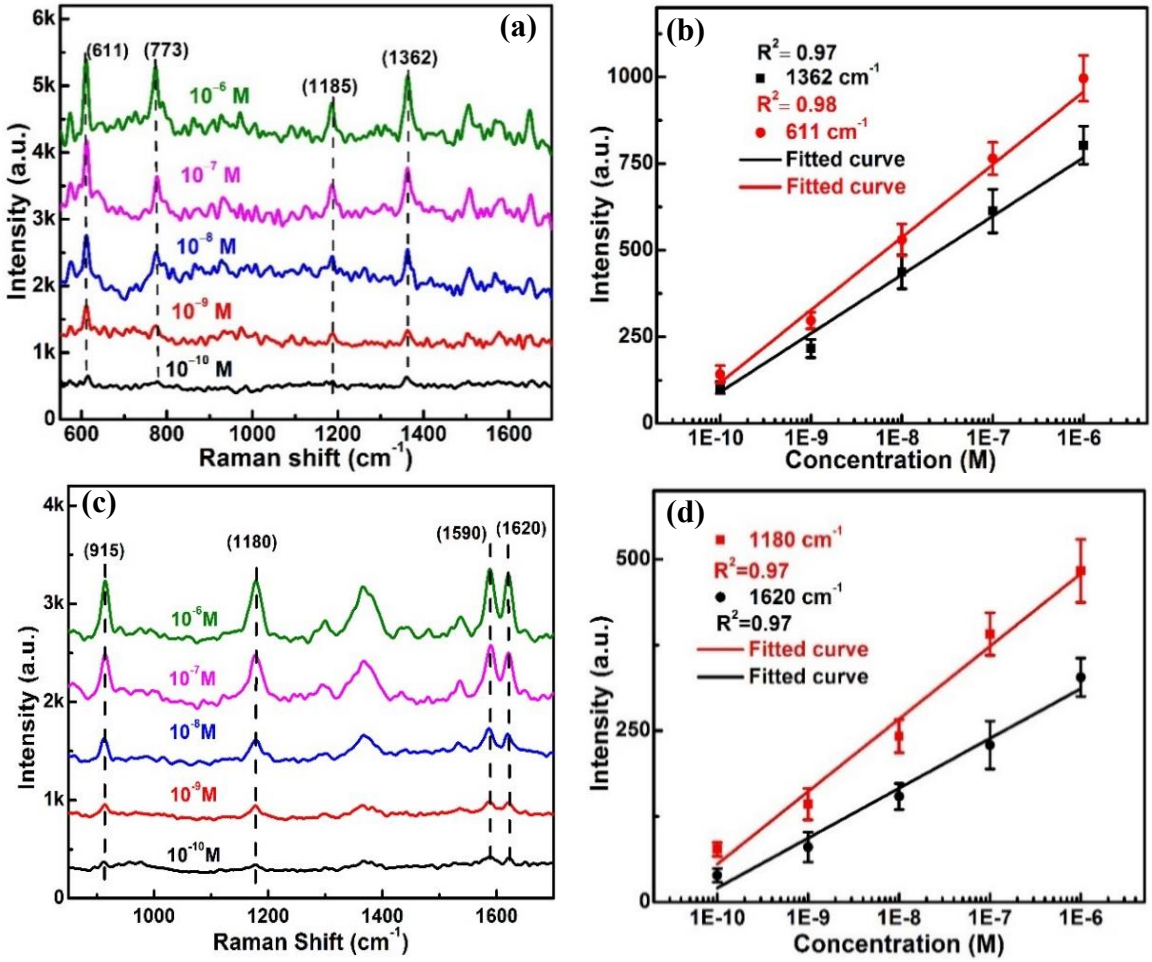

Figure 6.12 *SERS signals of (a) R6G and (c) MO dyes over VFL-MoS_2 at different concentrations. Raman intensity vs dye concentration of (b) R6G and (d) MO molecules for two different peaks.*

The significant intensities of SERS peak even at sub nano-molar (10^{-10} M) concentrations of both the dyes (R6G and MO) suggest the ultra-sensitive detection limit of prepared VFL-MoS_2/Si SERS substrate. This high detection efficiency of prepared SERS substrate can be attributed to the improved light absorption due to enhanced light trapping by multiple reflections between vertically oriented few-layer MoS_2 nanosheets [60, 207, 208]. Further, vertical orientation of interconnected few-layer MoS_2 nanosheets provides more accessible surface area for effective dye adsorption, which may lead to improved chemical mechanism [208, 209]. The chemical mechanism comprises of Herzberg-Teller vibronic coupling with molecular and excitonic resonances, as shown in

Figure 6.2. The quality of SERS performance can be calculated in terms of AEF using the **equation 6.1.** In the present case, AEF of 8.6×10^4 is observed for R6G using peak at 1362 cm^{-1}, while it is found to be 5.8×10^4 for MO using peak at 1180 cm^{-1}. In order to confirm the repeatability and uniformity, multiple SERS measurements were performed in different regions of the substrate for each concentration of both the dyes (R6G and MO) and obtained intensities of peaks have been incorporated in error bars of **Figure 6.12 (b, d)**. We have found that the VFL- MoS_2 shows highest detection limit up to 10^{-10} M of R6G and MO analyte molecule among pristine MoS_2 nanostructures. The higher detection efficiency of VFL-MoS_2/Si SERS substrate as compared to other reports on MoS_2 (**Table 6.1)** can be attributed to the enhanced light trapping by multiple reflections and higher accessible surface area for effective dye adsorption in VFL-MoS_2.

Table 6.1 Comparison of the SERS Detection Limit of Pristine MoS_2 Nanostructures.

SERS substrate	**Analyte**	**Detection limit**	**References**
Horizontal interconnected few-layer MoS_2	R6G	10^{-9} M	**Present Work**
Horizontally grown triangular bi-layer MoS_2	R6G	10^{-9} M	**Present Work**
Vertically oriented few-layer MoS_2	R6G and MO	10^{-10} M	**Present Work**
Horizontal MoS_2	R6G	10^{-6} M	Chem. Mater., 2016, **28**, 180−187.[120]
Horizontal MoS_2	R6G	10^{-6} M	Nanoscale, 2019, **11**, 485-494.[200]
Horizontal MoS_2	R6G	10^{-6} M	Small, 2014**, 10**, 1090-1095.[111]
3D-MoS_2 nanoflowers	RhB	10^{-7} M	J. Alloys Compd, 2020, **849**, 0925-8388. [124]

6.3 Conclusions

In summary, we have successfully synthesized and characterized three different MoS_2 based SERS substrates namely horizontally grown interconnected network of few-layer MoS_2/Si, horizontally grown triangular bi-layer MoS_2/SiO_2-Si and vertically oriented few-layer MoS_2/Si via CVD technique. We have demonstrated the SERS detection of R6G with horizontally grown MoS_2 based SERS substrates. The vertically grown MoS_2 shows detection of two dyes, R6G and MO. The efficient SERS detection using prepared MoS_2 may be attributed to the Herzberg-Teller vibronic coupling with molecular and excitonic resonances. Among studied SERS substrates in this work, VFL-MoS_2/Si shows best detection limit up to 10^{-10} M for both the dyes. It could be associated with better light absorption and dye adsorption in VFL-MoS_2 compared to other MoS_2 nanostructures.